Heliyon 6 (2020) e03857

Contents lists available at ScienceDirect

Heliyon

journal homepage: www.cell.com/heliyon

Research article

Mechanical properties of amorphous and semi-crystalline semi-aromatic polyamides

Stéphanie Djukic [a,*], Anthony Bocahut [b], Jérôme Bikard [b], Didier R. Long [a]

[a] LPMA, Laboratoire des Polymères et Matériaux Avancés, UMR 5268 Solvay/CNRS, Solvay in Axel'One, 87 avenue des Frères Perret CS 70061 69192 St-Fons Cedex, France

[b] Solvay Research and Innovation Center, 87 avenue des Frères Perret 69192 St-Fons Cedex, France

ARTICLE INFO

Keywords:
Materials science
Polyphthalamides
Polyamides
Mechanical properties
Strain hardening
Heliyon taxonomy

ABSTRACT

We investigate the mechanical properties of amorphous and semi-crystalline semi-aromatic polyamides, polyphthalamides (PPA). Three relaxation processes have been identified by DMTA which is consistent with literature for polyamide. PPA exhibit a brittle-to-ductile transition from a low impact strength to a high impact strength. At room temperature, all the studied PPA are brittle. During both tensile and compression experiments, a strain hardening behavior is observed for all the studied samples and is more pronounced in compression. The testing temperature has an influence on the strain hardening modulus, contrary to the crystallinity. Strain hardening gives properties of stability and resistance to damage.

1. Introduction

Polyamides are engineering thermoplastics which are useful for their high barrier properties. They are widely used in textile and automotive industries, where they compete with metals in a context of weight's reduction [1, 2, 3]. Polyamides are generally aliphatic and semi-crystalline. This is the case of PA 6, PA 66 or PA 6,10. Recently, polymers with different structures have been formulated to meet more technical applications. this is the case for example of semi-aromatic or fully-aromatic polyamides (MXDA, PA 6T/X, PA 10T/X, PA 10T [4]), and also amorphous polyamides [1], especially in order to improve the mechanical and thermal properties [5]. Polyphthalamides (PPA) are part of polyamide group. The main difference is the presence of aromatic rings in PPA's backbones, allowing them to have high mechanical and thermal resistance. PPA are synthesized by a reaction between aromatic acids (terephthalic acid or isophthalic acid) and aliphatic diamines (such as HMDA). If the PPA is mainly based on PA6T, the resulting PPA will be semi-crystalline [1]. PA6T is obtained by the reaction of terephthalic acid and HMDA. On the contrary, when the PPA is mainly based on PA6I (i.e. more than 55% of isophthalic acid), the resulting polymer will be amorphous [6]. This new class of polyamides has better properties compared to aliphatic polyamides (PA6 or PA66 [7] as an example), whether thermal (higher melting points and glass transition temperatures, better thermal stability), or chemical (better chemical resistance and lower water absorption). Few studies have been done for characterizing the properties of neat-PPA, such as thermal [8] or mechanical properties [9], but some studies exist on blends-based PPA or glass fiber reinforced PPA [10]. There is a need of more detailed data concerning mechanical properties. The study of the properties of this class of polymers is important, especially since their applications are different from aliphatic polyamides. PPA are used in several industries such as electronic devices, packaging or automotive industries. They can be used in composites for high temperature applications. PPA used in composites are mostly semi-crystalline because they maintain their properties at T_g, which is not the case of amorphous PPA. In this study, we will focus on the characterization of semi-crystalline and amorphous PPA. The ultimate mechanical properties and durability of polyphthalamides expected in applications such as automotive industry depend on the properties of strain hardening and impact strength [11]. Indeed, when dealing with ultimate mechanical properties the brittle-ductile transition T_{bd} is an essential notion to characterize, as well as the strain hardening regime. The strain hardening is generally interpreted as a result of a stress contribution of the orienting molecular network [11, 12, 13, 14, 15]. The objective of this paper is to study the ultimate mechanical properties of amorphous and semi-crystalline PA 6I/6T, through the study of the strain hardening and the brittle-to-ductile transition temperature. We consider three PPA, PA 6I/6T, with different proportions of PA6I or 6T, which gives the amorphous or semi-crystalline character of the polymer. The

* Corresponding author.
E-mail address: stephanie.djukic@gmail.com (S. Djukic).

https://doi.org/10.1016/j.heliyon.2020.e03857
Received 27 November 2019; Received in revised form 11 March 2020; Accepted 22 April 2020
2405-8440/© 2020 The Author(s). Published by Elsevier Ltd. This is an open access article under the CC BY-NC-ND license (http://creativecommons.org/licenses/by-nc-nd/4.0/).

viscoelastic properties in the linear regime will be studied by Dynamical Mechanical Thermal Analysis (DMTA). The yield stress σ_y and Young's modulus E measured by tensile tests, as well as the brittle-ductile transition temperature T_{bd} measured by both tensile and Charpy impact tests are determined for the considered PPA samples. The strain hardening in compression is studied.

2. Experimental methods

2.1. Materials

Three semi-aromatic polyamides were considered. Figure 1 shows the structure of the copolymer PA6I/6T. Polymers are formed by copolymerization of the PA6T and PA6I in different proportions. Monomers are obtained by the condensation reaction of hexamethylenediamine (HMDA) with a diacid: isophthalic (terephthalic) acid for the PA6I (PA6T) monomer. The resulting PPA can be amorphous or semi-crystalline depending on the combination of the monomers [1]. Semi-crystalline PPA are mainly based on PA6T, while the resulting copolymer is amorphous if there is more PA6I [6]. Each PPA corresponds to a different fraction in PA6I or PA6T, indicated in Table 1.

The number-average and weight-average molecular weight M_n and M_w were determined by Size Exclusion Chromatography (SEC). M_n is around 10000 g mol^{-1} for Polyamide A and B and around 6000 g mol^{-1} for Polyamide C whereas PPA whereas M_w is around 30000 g mol^{-1} for Polyamide A, B and C. M_n and M_w were used to calculate the polydispersity index I_p (see Table 1). As explained by Martins et al [16], secondary reactions may occur during polymer synthesis. These secondary reactions lead to branched chains in small proportions and, possibly, may explain why the polydispersity index varies from 3.0 to 5.1 [16]. As observed in Table 1, the values of polydispersity are larger than 2, which is the value expected by Flory's theory for linear polycondensation [16,17].

The glass transition temperature T_g was determined by Differential Scanning Calorimetry (DSC). T_g is similar and about 130 °C. Like all semi-aromatic PPA with more than 55% of PA6I [6], Polyamide A is amorphous. Polyamide B and C are both semi-crystalline, with a crystallinity ratio of 4.3% and 16.4%, respectively. Crystalline fractions were calculated using the following formula (Equation 1):

$$\chi_c = \frac{\Delta H_f^{measured}}{\Delta H_f^{100\%}} \tag{1}$$

where $\Delta H_f^{100\%}$ is the enthalpy of melting of a 100% crystalline polymer.

It can be found in literature for PA6,6 (188 J g^{-1} [18]) and PA6,10 (207 J g^{-1} [18]), but not for the crystalline PA6T part of Polyamide C. As a consequence, an average value of 200 ± 20 J g^{-1} is commonly used [19]. To provide a better estimation of the crystalline fraction, $\Delta H_f^{100\%}$ value for the PA6T was determined by WAXS (Wide-Angle X-ray Scattering) experiments. The peaks obtained in WAXS were deconvolved and the amorphous halo was subtracted from the crystalline peaks. The crystalline fraction χ_{RX} was calculated using Eq. (2):

$$\chi_{RX} = \frac{A_C}{A_C + A_A} \times 100 \tag{2}$$

with A_C and A_A the areas of crystalline and amorphous parts, respectively.

Then the enthalpy of melting of a 100% crystalline PA6T is calculated as follow (Equation 3):

$$\Delta H_f^{100\%} = \frac{\Delta H_{DSC}}{\chi_{RX}} \tag{3}$$

For a 100% crystalline PA6T, the enthalpy of melting is 196 J g^{-1}. An Oxford Xcalibur Mova diffractometer was used in transmission mode in order to record WAXS data. Measurements were performed at the Henri Longchambon Diffraction Center of University of Lyon.

2.2. Injection molding

Polymers were injection-molded into tensile and impact strength specimens with a Billion select 100T injection press. Prior to molding, water content has been controlled by Karl Fischer in order to avoid hydrolysis or post-condensation reaction. Higher water content leads to hydrolysis and the molecular weight decreases. If the moisture content is lower than that of the chemical equilibrium, a post-condensation reaction with water formation and an increase of the molecular weight of the resulting polyamide may occur. Pellets were dried 24 h at 110 °C under vacuum before processing. Mold temperature was kept at 30 °C. After molding, the samples were stored in sealed bags to maintain them dry. Tensile and impact strength specimens dimensions were 150 × 10 × 4 mm^3 and 80 × 10 × 4 mm^3 respectively (ISO-527 and ISO-157 norms) (see Figure 2-1 for tensile geometry and Figure 2-2 for impact strength geometry). In Table 2, we gather the processing conditions of our samples.

The injection process has an influence on mechanical properties of polymers, in particular on the skin-core effect due to flow during injection [20]. This effect is present in the industrial process, due to a temperature gradient between the mold and the polymer melt (at higher temperature) during the injection process. A skin-core effect was observed for Polyamide C by cross-polarized optical microscopy. Indeed, a birefringent character was observed between the skin and the core of the polymer. Samples of Polyamide C were injection-molded with different mold temperatures (30, 60, 80 and 100 °C). The storage modulus E′ determined by DMTA shows no difference regardless of the mold temperature (E' = 3.1 GPa at 25 °C for the four mold temperatures). The temperature of the mold during the injection has no impact on the modulus E'. The degree of crystallinity remains low and is homogeneous over the thickness for the two semi-crystalline PPA (Polyamide B and Polyamide C), and was verified by DSC experiments. The skin-core effect observed for Polyamide C only is related to shearing during the injection process and not to a difference in crystallinity within the material. The choice of setting the mold temperature at 30 °C corresponds to an internal injection process and has no impact on our results.

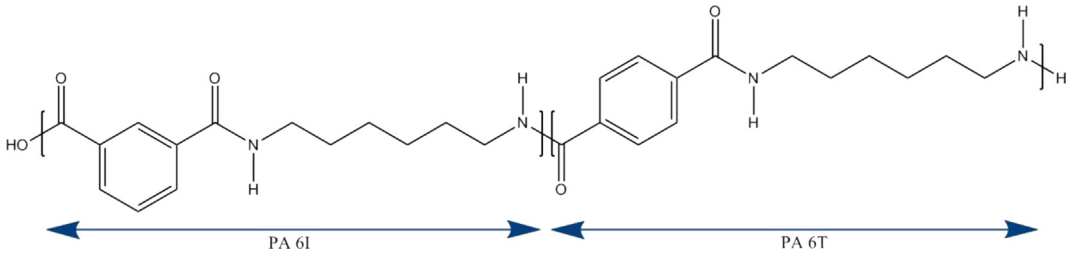

Figure 1. Structure of the copolymer PA6I/6T.

Table 1. List of studied semi-aromatic polyamides and corresponding molecular weight distribution (number-average M_n and weight-average Mw, polydispersity index ($I_p = M_w/M_n$) determined by Size Exclusion Chromatography (SEC) in PMMA equivalents), glass transition T_g and melting temperatures Tm determined by Differential Scanning Calorimetry (DSC), crystallinity ratio determined by Wide Angle X-Ray Scattering (WAXS). All the samples were dried as molded (d.a.m.).

		M_n (g mol^{-1}) (±5%)	M_w (g mol^{-1}) (±2.5%)	$I_p = M_w/M_n$	Crystallinity (%) (d.a.m.)	T_g (°C)	T_m (°C)
Polyamide A	PA6I/6T 70/30	9356	27963	3.0	0	129.2	/
Polyamide B	PA6I/6T 50/50	10424	32917	3.2	4.3	129.3	265
Polyamide C	PA6I/6T 30/70	6450	32779	5.1	16.4	132.4	319

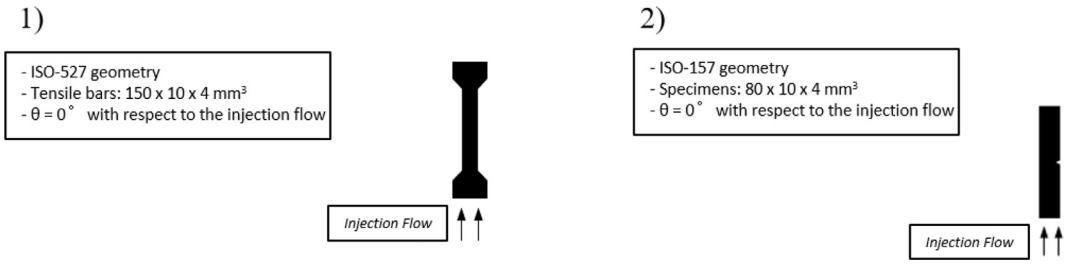

Figure 2. Tensile geometry of the specimens (1) and impact strength geometry of the specimens (2).

2.3. Characterization methods

2.3.1. Differential scanning calorimetry (DSC)

The characteristic temperatures (glass transition, melting and crystallization temperatures) of the studied polymers were characterized by differential scanning calorimetry (DSC). A TA Instruments Q2000 calorimeter was used in the standard mode. For each measurement, non-hermetic aluminum pans were filled with 5–10 mg of polymer sample. Thermal measurements were performed at a heating/cooling rate of 10 °C min^{-1}, under a nitrogen gas flow (50 mL min^{-1}). Samples were first annealed from 40 to 350 °C, then cooled down to 40 °C and finally heated again to 350 °C. Glass transition and melting temperatures were measured from the second heating cycle. The glass transition temperature was determined at the onset. Crystalline ratios of the sample were calculated as discussed above.

2.3.2. Dynamic Mechanical Thermal Analysis (DMTA)

Dynamic Mechanical Thermal Analysis (DMTA) allows studying the viscoelastic properties of a material by measuring its dynamical modulus at a given frequency as a function of temperature [21]. Experiments were carried out in the field of linear behavior, with a deformation between 5 × 10^{-3} % and 0.01%. A TA Instruments RSA-G2 device, equipped with a three-point bending geometry was used. The samples were injected in the form of bars (Charpy impact specimens) then cut with a saw. Polymer samples dimensions were $40 \times 10 \times 4\ mm^3$. Measurements were performed at fixed frequencies of 0.1 Hz, 1 Hz, 10 Hz, 50 Hz and 75 Hz with a temperature sweep of -150 °C–150 °C, at a rate of 2 °C min^{-1}. The laboratory was at a controlled temperature (23 °C) and hygrometry (RH 50). The studied PPA were dried as molded (d.a.m.), the temperature equilibration time was too small to induce significant water intake. Each DMTA measurement was carried out twice for each frequency. The temperature corresponding to each relaxation was determined as the maximum of the relaxation peak observed in the loss modulus E″ plot, as described in the standard ASTM D5023.

2.3.3. Impact strength

In order to obtain the resilience of the studied polymers as well as to characterize their brittle-to-ductile transition temperature, T_{bd} at high speed (impact conditions), Charpy impact measurements were performed. The setup consists in a CEAST 9050 Instron classic Charpy pendulum equipped with a 7.52 J-energy hammer. The polymer samples, with a dimension of 80 × 10 × 4 mm^3 were notched with a notch radius of 0.25 mm and a notch depth fixed at 2 mm. Each sample was hit at a speed $\nu_{impact} = 3.8\ m\,s^{-1}$, which corresponds to a deformation rate of $\nu_{impact}/r_{notch} = 1.5\ .10^4 s^{-1}$. In order to obtain the brittle-ductile transition temperature T_{bd} of the studied polymers, the impact strength tests were performed in a temperature range from -40 °C to 230 °C. Samples were kept in a thermally controlled chamber and were conditioned for 15 min at the set temperature for equilibrium before being tested. The temperature of the samples was considered to remain constant during the impact tests. The laboratory was at a controlled temperature (23 °C) and hygrometry (RH 50). The studied PPA were dried as molded (d.a.m.), the temperature equilibration time was too small to induce significant water intake. Ten specimens were tested at each temperature. The resilience (J m^{-2}) was calculated by dividing the energy used to fracture the sample by the fracture surface area under the notch [22].

2.3.4. Video-controlled tensile test

In order to characterize the Young modulus E, the yield stress σ_y and the brittle-ductile transition temperature T_{bd} of the studied PPA, tensile strength experiments were carried out on a Zwick/Roell Z050 universal testing machine equipped with a 50 kN load cell, a thermally controlled chamber and a non-contact extensometer (VidéoTraction®) [23], equipped with two cameras. The VidéoTraction® system measures the

Table 2. Injection conditions for ISO-527 (Tensile) and ISO-157 (Choc) geometries.

	Temperatures (°C)		Molding cycle time (s)	
	Screw			
	Choc specimens	Tensile specimens	Choc specimens	Tensile specimens
Polyamide A	280	280	36.43	45.26
Polyamide B	290	290	41.32	47.24
Polyamide C	330	330	33.36	33.18

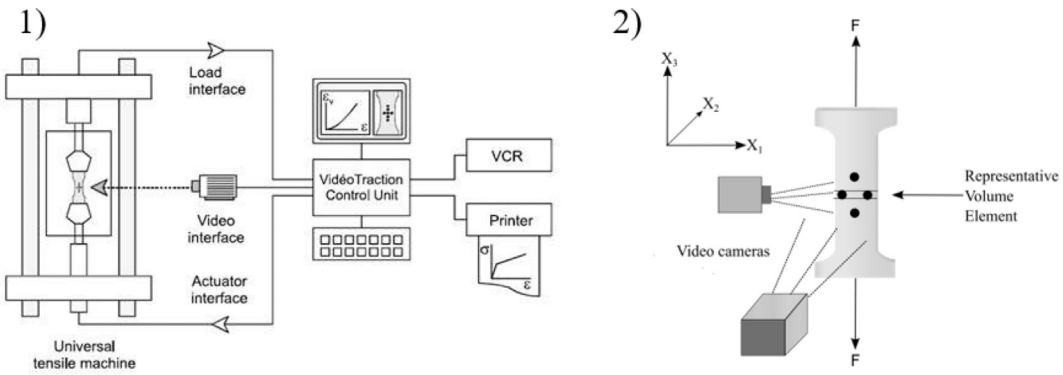

Figure 3. Representation of the VideoTraction® system (1) and the markers on the middle of the tensile specimen with the two cameras (2). Adapted from [23] with permission from Elsevier.

true strain and the true stress during the test, in a representative volume element. The representative volume element can be defined by several dot markers placed in the middle of the tensile specimen. The development of localization phenomena like necking is taken into account in the measured behavior [24]. In the studied samples, the necking area is reproducible. The dot markers are placed in order to study this area. Samples were dried as molded (d.a.m.) and were strained at a constant strain rate $\dot{\varepsilon} = 1.10^{-3}s^{-1}$ at different temperatures (between -40 °C to 160 °C). The lower temperature of chamber is -40 °C. Each sample was conditioned 20 min in the temperature chamber before being tested. For each temperature, five samples were tested.

The nominal strain ε_n is given by Eq. (4):

$$\varepsilon_n = \frac{\Delta l}{l_0} = \frac{l - l_0}{l_0} \tag{4}$$

with l the length at each time t and l_0 the initial length of the specimen.

The nominal stress σ_n can be expressed as:

$$\sigma_n = \frac{F}{S_0} \tag{5}$$

with F the force acting on the specimen and S_0, the initial cross sectional area.

At large deformations, amorphous polymers have a high ductility. During the tensile test, the sample cross sectional area is not constant. The instantaneous cross sectional area S(t) should be used instead of S_0. The videoextensometer gives access to the elastoviscoplastic response of polymers under uniaxial tension. Local measurements of true strains are performed at the center of the neck (see Figure 3) [23]. Four dot markers are printed on the front face of the sample prior to deformation, within a representative elementary frame. The thickness deformation is also measured allowing to calculate S(t) for each value of l(t). Local deformations are measured between the dots and the true strain ε_v is related to the nominal strain and the elongation ratio λ by the following equation [25]:

$$\varepsilon_v = ln\left(\frac{l}{l_0}\right) = ln\left(1 + \frac{l - l_0}{l_0}\right) = ln(1 + \varepsilon_n) = \ln(\lambda) \tag{6}$$

The true strain rate $\dot{\varepsilon_v}$ is defined as:

$$\dot{\varepsilon_v} = \frac{\dot{l}}{l(t)} \tag{7}$$

with $\dot{l}$ the velocity of elongation and l(t) the length at each time t.

The true stress σ_v is obtained and is given by Eq. (8).

$$\sigma_v = \frac{F}{S(t)} = \sigma_n \frac{S_0}{S(t)} \tag{8}$$

Thanks to the two cameras, the VideoTraction system makes it possible to determine the barycenter of each marker drawn on the specimen and calculate their relative displacements (Figure 3). Thus, the system calculate simultaneously in-plane and out-of-plane deformations.

2.3.5. Compression

Compression tests were performed on a Zwick/Roell Z050 universal testing machine equipped with a 50 kN load cell, a thermally controlled chamber and a non-contact extensometer (VidéoTraction®) [23]. The geometry of the sample is an important limitation of this test. Cubes of dimensions $10 \times 10 \times 4\ mm^3$ were cut in the ISO-527 tensile specimens. It is necessary to avoid the barreling or buckling of the sample [26]. The friction has been reduced by lubrification of the plate to prevent the buckling of the sample. Thanks to VidéoTraction®, we could check that there is no barrel nor buckling. It allows us to consider the friction as negligible in the test and then the compression field homogeneous all over the specimen.

Specimens were compressed at a constant strain rate $\dot{\varepsilon} = 1.10^{-3}s^{-1}$ between two parallel flat steel plates. Tests were performed at different temperatures, from -20 °C to 120 °C. Each sample was conditioned 20 min in the temperature chamber before being tested. For each temperature, five samples were tested.

For the analysis of the strain hardening response, the compression curves were plotted versus the Green-Lagrange strain [27]:

$$g(\lambda) = \lambda^2 - \lambda^{-1} \tag{9}$$

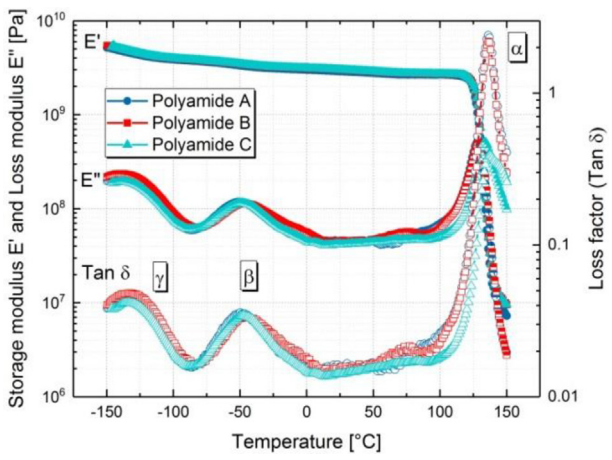

Figure 4. Temperature dependences of the storage modulus E′, the loss modulus E″ and the damping factor tanδ, as determined at 1 Hz for the different PPA by DMTA measurements. The different relaxation processes are indicated on the tanδ curves.

Table 3. Temperatures of the different relaxations, α, β and γ for each polymer determined at 1 Hz.

Copolyamides	T_α (°C)	T_β (°C)	T_γ (°C)
Polyamide A	128.2	-51.7	-140.6
Polyamide B	129.3	-46.7	-139.6
Polyamide C	134.3	-48.6	-137.6

The strain hardening modulus, E_{SH}, was determined from the slope of the curves in the strain range $1.75 \geq g(\lambda) \geq 1.25$.

3. Results and discussion

3.1. Thermo-mechanical properties

Temperature sweep measurements were performed at frequencies of 0.1, 1, 10, 50 and 75 Hz. The temperature of each relaxation was determined as the maximum of the relaxation peak observed in the loss modulus E″ plot. To determine correctly the characteristic temperature of each relaxation process, a Gaussian function was used to fit each peak, and therefore determined the peak maximum. At 23 °C and 1 Hz, the storage modulus E' is high and is 2.92 GPa for Polyamide A, 3.01 GPa for Polyamide B and 2.96 GPa for Polyamide C, which is comparable with others polymers (2.5 GPa for poly(phenylene oxide) PPO and 3 GPa for polystyrene PS) [12]. PA66, which is an aliphatic polymer, has an elastic modulus of 2.8 GPa, measured at 23 °C at 1 Hz, which is comparable to the elastic modulus of our samples [28,29]. The differences observed in elastic moduli are not significant. Indeed, the two semi-crystalline PPA have the same behavior as the amorphous PPA, with a module of 3 GPa. The crystallinity has no influence in our case.

The temperature dependences of the storage modulus E' and the damping factor tanδ, as determined at 1 Hz for the different PPA are shown in Figure 4.

Starting from low temperature, the storage modulus E' reduces slowly and decreases strongly at the glass transition temperature T_g.

In addition to the final relaxation process (α) we observe two peaks on tanδ for each polymer, denoted γ and β. Indeed, three relaxations processes have been identified in other semi-aromatic and aliphatic polyamides [30, 31, 32, 33] by DMTA and by broadband dielectric spectroscopy (BDS) [34,35].

At the lowest temperature, the γ-relaxation is generally assigned to local motions of short aliphatic sequences -$(CH_2)_n$-internal to the monomer for aliphatic polyamides [30,36]. This relaxation is observed around -140 °C at 1 Hz, which is comparable to the γ-relaxation observed by Varlet et al [36] for PA 12. The β-relaxation is associated to the rotation of amide groups (-NHCO-) along the polyamide chain, and is observed around -50 °C at 1 Hz. The α-relaxation corresponds to segmental movements (several monomers). This main relaxation is observed at high temperature and is close to the glass transition temperature measured by DSC. The temperatures T_α, T_β and T_γ determined by DMTA at 1 Hz for the three PPA, are listed in Table 3. As shown by the data displayed in Table 3, the increase in PA6T content induces a slight increase of the α-relaxation temperature of 6 °C, which is also observed in literature for other polyamides [30,37]. A weak and wide shoulder is also observed in our measurements around 70 °C and can be associated with departure of water [31,33]. As measured by Karl Fischer, our polymers contain about 700 ppm of water. A departure of water contained in the polymer causes a shift of the relaxation towards high temperatures.

3.1.1. Time/temperature dependence of relaxations

From the DMTA curves obtained at different frequencies (0.1, 1, 10, 50 and 75 Hz), we plot the time/temperature dependence of the γ, β and α relaxations processes $log\tau = f(1000/T)$ for each polymer in Figure 5.

The main relaxation, α, follows the Williams-Landel-Ferry equation (WLF) [38] defined as follow [39]:

$$\log(a_T) = \frac{-C_1(T - T_{ref})}{C_2 + T - T_{ref}} \tag{10}$$

with C_1 and C_2 the WLF constants. T_{ref} is the reference temperature defined as 300 K and is and is chosen arbitrarily.

Secondary relaxations, γ and β, were fitted through an Arrhenius law:

$$\tau(T) = \tau_0 exp\frac{E_A}{RT} \tag{11}$$

with E_A, the activation energy, τ_0 the characteristic time, R the ideal gas constant and T the temperature. Using the values obtained in the Arrhenius fit, the entropy related to each relaxation can be calculated (using this relation: $\tau_0 = \tau_{Debye} exp\frac{\Delta S}{R}$). From this value, the free energy ΔG can be calculated for each relaxation at a reference temperature T_0 of 300K ($\Delta G = E_A - T_0\Delta S$). Table 4 shows the activation energy E_A, the

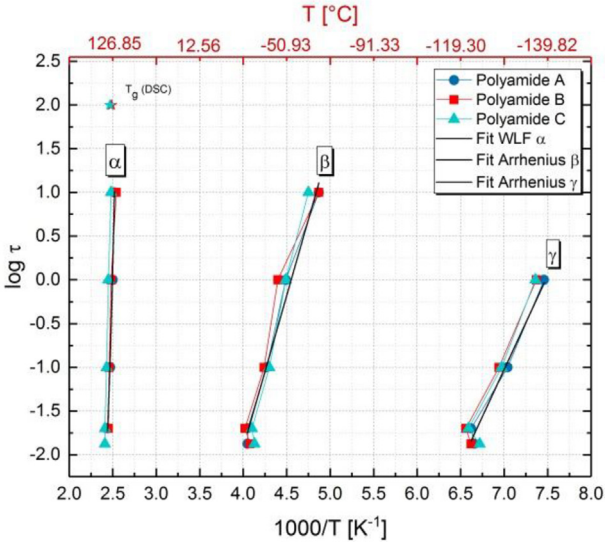

Figure 5. Time/temperature dependence of relaxations for the three PPA. From left to right, the different relaxations are shown: α, β and γ, as well as the T_g determined by DSC.

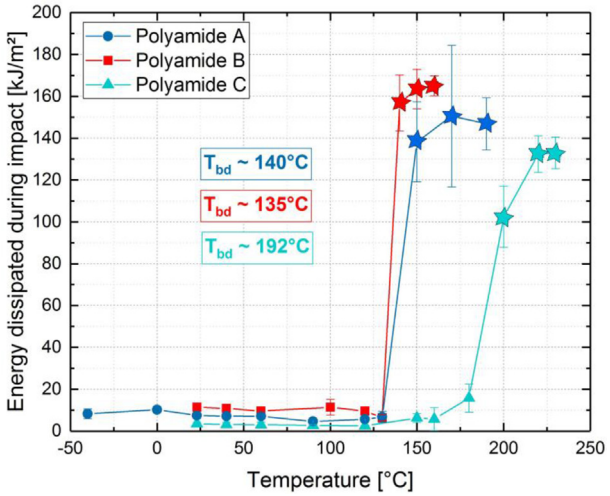

Figure 6. Brittle-ductile transition curves of all the PPA samples obtained from Charpy impact measurements. Evolution of the energy dissipated by the material with the temperature and the brittle-ductile transition temperature T_{bd}. The stars represent the unbroken samples above the T_{bd}.

Table 4. Activation energy E_A, characteristic time at infinite temperature τ_0, entropy -TγΔS and -TβΔS and free energy ΔG of the γ and β relaxations for each PPA.

Polymer	ã-relaxation				â-relaxation			
	E_A (kJ mol^{-1})	ô$_0$ (s)	- T$_a$ÄS (kJ mol^{-1})	ÄG (kJ mol^{-1})	E_A (kJ mol^{-1})	ô$_0$ (s)	- T$_a$ÄS (kJ mol^{-1})	ÄG (kJ mol^{-1})
Polyamide A	41.16	$10^{-16.1}$	10.35	17.75	66.5	$10^{-15.8}$	15.62	45.4
Polyamide B	43.37	$10^{-16.7}$	12.05	16.3	66.04	$10^{-15.6}$	15.71	45.2
Polyamide C	46.66	10^{-18}	15.48	12.4	85.06	10^{-20}	34.65	38.7

Table 5. WLF fitting parameters for the α–relaxation.

Copolyamides	C_1^g	C_2^g(K)
Polyamide A	1.81	134.68
Polyamide B	1.81	134.78
Polyamide C	1.77	137.88

characteristic time τ_0, the entropy -TΔS and the free energy ΔG of the γ and β relaxations for each PPA.

3.1.2. Secondary relaxations

For the γ relaxation, the activation energy E_A is in the range of 40 kJ mol^{-1} (from 41 to 46 kJ mol^{-1}). This range of activation energy was reported in literature by several authors for aliphatic polyamides or semi-aromatic copolymers based on PA 6I [31,33,40]. The expected value for the prefactor τ_0 is 10^{-12} s, which is the Debye time ($\tau_{Debye} = 10^{-12}$ s [41]) if there is no contribution to the free energy barrier. This is not the case here, since the prefactor τ_0 is smaller than this value. Very small relaxations time values are an indication of an entropic contribution. Note that Laurati et al and Laredo et al have observed in the presence of water smaller values of τ_0, close to the values determined for our polymers (see Table 4) [31,33].

The value of ΔG (about 17 kJ mol^{-1}) for polyamides A and B are identical to the value corresponding to the rotational barrier for the C–C torsion motion [42,43].

In the case of the β-relaxation, for the amorphous PPA, Polyamide A, the free energy ΔG is 45.4 kJ mol^{-1}. This value is in good agreement with the value determined by Bocahut et al for the free energy barrier associated to the rotation of amides groups ($\Delta G = 40 \pm 5$ kJ mol^{-1}) [44].

Note that the entropy ΔS of Polyamide C is twice the entropy of polyamides A and B. Small values of ΔS for polyamides A and B indicate that the motions responsible for the β-relaxation are very localized modes [30,37]. On the contrary, the entropy ΔS is twice for Polyamide C, based mainly on terephthalic acid, which is an indication that the motional cooperativity is higher [30].

3.1.3. Main relaxation α

The α-relaxation can be fitted using the WLF equation mentioned above (Equation 10). The WLF constants C_1 and C_2 were respectively 7.54 and 32.33K, for the three PPA. Because of the dependency in frequency and temperature of E', a time-temperature superposition curve (tTS) can be established for Polyamide A. The shift factor a_T can be fitted with the WLF equation. C_1 and C_2 WLF constants are respectively 17.62 and 71.98K [39,45]. C_1 and C_2 WLF constants are reported to T_g with Eqs. (12) and (13) [46]:

$$C_1^g = \frac{C_1 C_2}{C_2 + T_g - T_{ref}} \tag{12}$$

$$C_2^g = C_2 + T_g - T_{ref} \tag{13}$$

Where C_1 and C_2 are the WLF constants, T_g is the glass transition temperature determined by DSC for each polymer and T_{ref} is the arbitrary chosen reference temperature defined as 300 K.

The WLF constants C_1^g and C_2^g are reported in Table 5. No significant difference was observed in the WLF constants.

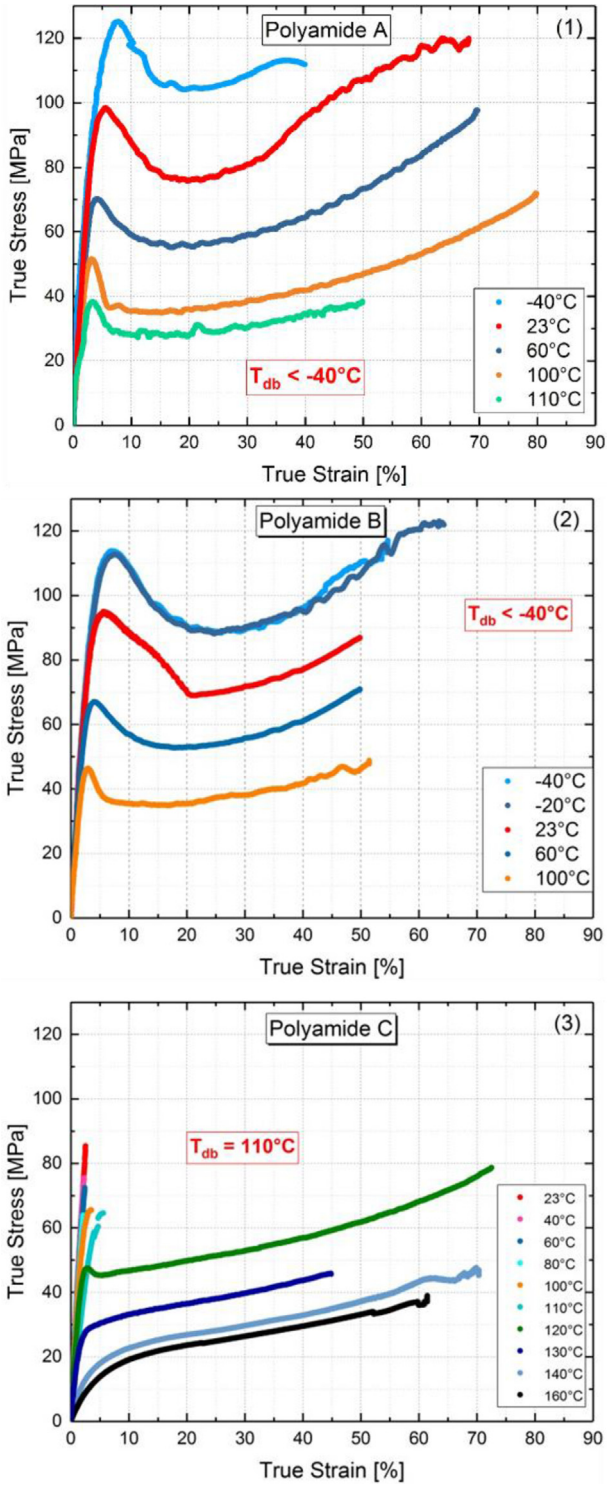

Figure 7. Uniaxial tensile true stress-true strain curves determined for Polyamide A (1), Polyamide B (2) and Polyamide C (3) at several temperatures and a strain rate of 1.10^{-3} s^{-1}.

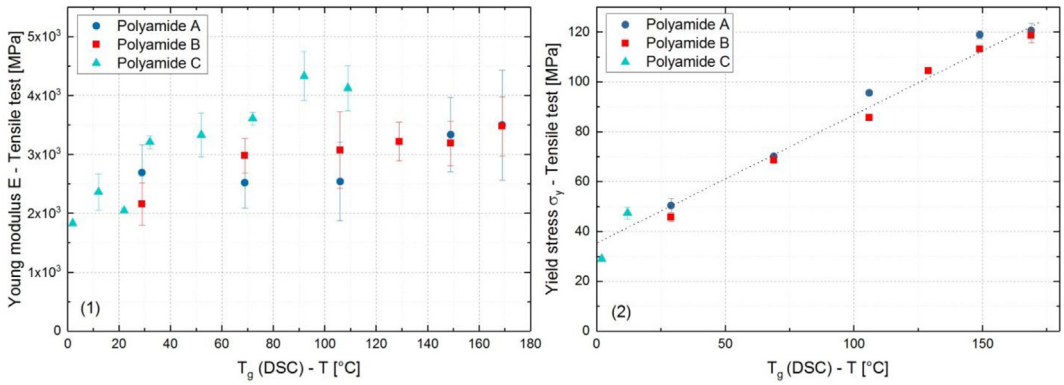

Figure 8. Evolution of the Young modulus E (1) and the yield stress σ_y (2) as a function of T_g-T. Data are obtained from tensile measurements at a constant strain rate of 1.10^{-3} s^{-1}.

3.2. Characterization of the brittle-ductile transition T_{bd}

3.2.1. Charpy impact strength

The transition from brittle to ductile, denoted T_{bd}, may be characterized by Charpy impact test or in uniaxial tensile experiments. Charpy impact test is a dynamic test at a frequency of 10^3 Hz. Impact strength tests are conducted on all the studied samples as described in the experimental section. Figure 6 shows the energy dissipated during impact as a function of temperature (brittle-to-ductile transition curves) for all the studied samples. At low temperatures, all samples show a brittle failure with an impact strength varying from 3 to 11 kJ m-2. At high temperatures, the specimens do not break and present a ductile behavior. A well-defined transition from brittle to ductile behavior is observed for all polymers. A large region of plastic deformation close to the tip of the tail is observed. Specimens evolve from a fragile elastic behavior to a ductile plastic behavior. A brittle-ductile transition can be determined for the three PPA (Figure 6). For the amorphous polymer, Polyamide A, the T_{bd} is equal to 140 °C. For the low semi-crystalline PPA, Polyamide B, the T_{bd} is close, 135 °C. For these two polymers, we can see that this transition T_{bd} is very close to the glass transition T_g determined by DSC (see Table 1). We observe that the brittle-ductile transition temperature is higher for the PPA with the largest crystalline fraction, Polyamide C (192 °C).

The same behavior is observed for different PA6,6 with a well-defined brittle-ductile transition with a resilience at low temperature of order 2–5 kJ m^{-2} [47,48]. At high temperature, the resilience of the PA6,6 is of order 60 kJ m^{-2}, which is lower than for the studied PPA. The brittle-ductile transition temperature of RT-PMMA (rubber-toughened PMMA) is about 20 °C, which is very low compared to the studied PPA [49].

The energy dissipated during impact in the ductile regime at 150 °C is high (from 130 to 160 kJ m^{-2}). The brittle-ductile transition temperature is also very high for the three PPA.

3.2.2. Influence of frequency on T_{bd}

The brittle-ductile transition temperature T_{bd} at lower frequency is observed in uniaxial tensile experiments as the temperature at which failure occurs at the yield stress σ_y [25]. The true stress-true strain curves obtained from tensile experiments at different temperatures are presented in Figure 7 for the three polyamides. When the temperature decreases, the rigidity of the polymer increases. A transition from ductile to brittle behavior can be observed in Figure 7. Below 110 °C, Polyamide C is brittle, the sample breaks before reaching the yield stress σ_y. When the temperature increases, the mobility of the chains is accelerated and a yield point can be determined, as observed for Polyamide A and B, and above 110 °C for polyamide C (in Figure 7-3). As explained above (see 3.2.1), the behavior goes from brittle to ductile. The temperature T_{bd} is defined for Polyamide A and Polyamide B below -40 °C. For Polyamide C, T_{bd} is clearly visible and is determined at 110 °C. Because of the limitation of the temperature of the temperature chamber, we cannot perform tensile tests below -40 °C. Contrary to the Charpy impact strength described in the previous paragraph, the tensile test is a quasi-static test at a frequency of 10^{-3} Hz. We can emphasize the influence of the frequency on this temperature: the higher the frequency, the higher the temperature T_{bd}. As for the Charpy impact test, the brittle-ductile transition temperature is strongly influenced by the crystallinity and is higher for the most semi-crystalline PPA, Polyamide C (192 °C).

3.3. Tensile behavior

Figure 7 represents the true stress-true strain curves obtained from tensile experiments for the three polyamides. The behavior of all samples is essentially the same. Beyond the yield point, a strain softening regime is observed. It corresponds to a stress decrease with increasing deformation [50]. The strain softening is followed by a strain hardening regime.

The strain hardening behavior is also observed in others amorphous polymers such as cellulose acetate, PC, PMMA or PVC [12, 51, 52, 53]. It can be defined as a stress increase at large strains. The strain hardening modulus E_{SH} is defined as the slope at large strains. The three PPA studied have a very ductile behavior. Beyond the brittle-ductile transition T_{bd}, the failure takes place at a deformation larger than the deformation accessible within the testing machine, which is a limitation for the study of strain hardening.

The equations mentioned so far apply when a polymer exhibits uniform deformation (see Equations (4),(5),(6),(7) and (8)). Beyond the plasticity threshold, several polymers (such as PC, PE, PVC, PP or PA) [25, 54, 55, 56] show deformation heterogeneities called necking. This phenomenon is related to a local stress concentration (due to a variation of section) which makes the deformation field non-uniform within the sample. The appearance of this phenomenon is a consequence of a mechanical instability due to a strain softening. Strain softening is stabilized by strain hardening. In tensile test, further studies shown that the strain hardening regime is influenced by the temperature, the polymer chains orientation and the geometry of the sample [51,57]. The study of strain hardening will be detailed in the case of the compression test. The strain softening amplitude is larger at low temperatures than at high

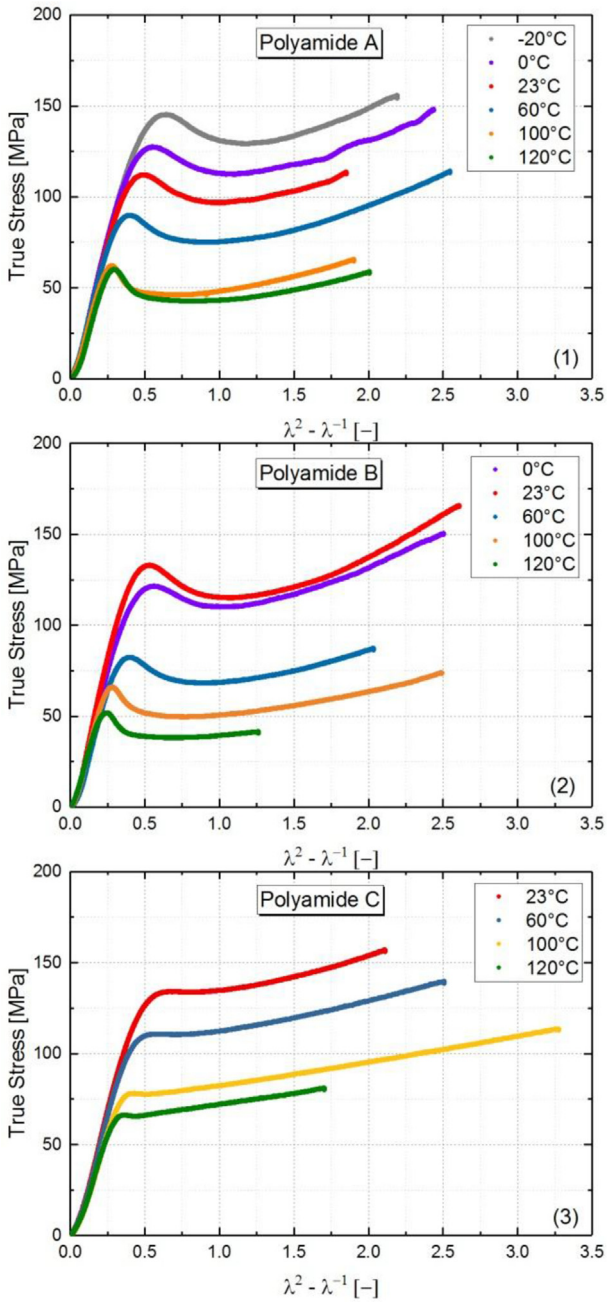

Figure 9. Compressive behavior of PPA at several temperatures at strain rate of 10^{-3} s^{-1}. (1) Polyamide A, (2) Polyamide B and (3) Polyamide C.

temperatures, which is similar to the behavior observed for PMMA or PC [54,58].

3.3.1. Evolution of the young modulus E and the yield stress σ_y

The Young modulus E is calculated from the tangent line in the elastic domain (between 0.05 and 0.25% of true strain) and the yield stress σ_y is defined as the observed maximum stress.

Figure 8 shows the evolution of the young modulus (Figure 8-1) and the yield stress (Figure 8-2) as a function of T_g-T. This representation makes it possible to compare the 3 PPA at a given state of molecular mobility. Young modulus E and yield stress σ_y values are reported for temperatures below the glass transition temperature T_g. No particular

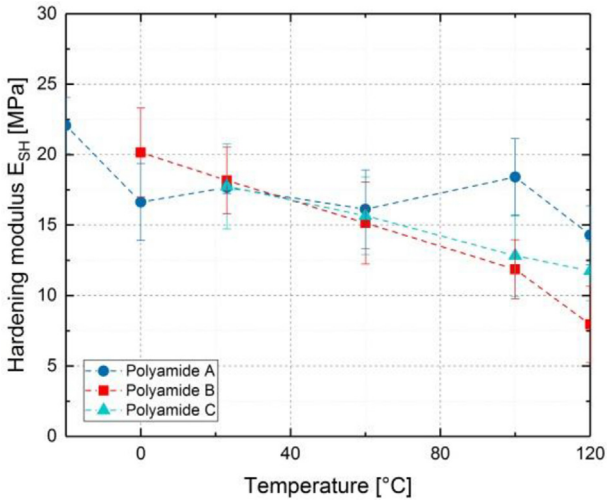

Figure 10. Evolution of the hardening modulus E_{SH} in compression with the temperature for each PPA. The modulus E_{SH} was determined from the slope of the curves in the strain range 1.25–1.75.

relation appears for the Young Modulus E when plotted as a function of T_g-T, whereas the yield stress σ_y fall on a linear master curve. The Young Modulus E of the studied PPA is much higher than that of a PA66, which is an aliphatic polyamide. Indeed, the PA66 has a Young Modulus E of the order of 1100 MPa (at room temperature and 10 mm min^{-1}) [48].

3.4. Compression behavior

The true stress-true strain curves obtained in tensile tests present a necking phenomenon. We performed uniaxial compression tests to avoid localization phenomena at large deformation. We plot the true strain as $(\lambda^2 - \lambda^{-1})$, which is a standard representation for the study of the strain hardening and often used in literature [12,27].

Figure 9 shows the results plotted as true stress versus $(\lambda^2 - \lambda^{-1})$ for the three polyamides at several temperatures. A moderate strain softening followed by a strain hardening results in a macroscopic ductile behavior [59].

The strain softening is more pronounced for the amorphous PPA. Indeed, The strain softening is an amorphous property [60] and increasing the crystallinity seems to result in a decrease in strain softening.

Figure 10 shows the evolution of the strain hardening modulus E_{SH} determined from the true stress – $(\lambda^2 - \lambda^{-1})$ curves with the temperature for each polymer. Values of hardening modulus are shown in Table 6. The strain hardening modulus is similar for the three PPA. The strain hardening modulus of the semi-crystalline PPA is found to be equal to that of the amorphous PPA and is clearly not related to the degree of crystallinity. This was observed in literature by Schrauwen et al with different semi-crystalline polymers (polyethylene, polypropylene and poly(-ethylene terephthalate)) [61]. At room temperature, the strain hardening modulus E_{SH} for the three PPA is about 18 MPa. It is larger than the strain hardening modulus of PS (13 MPa) [12] but smaller than other amorphous polymers (at room temperature, E_{SH} of PC, PPO and PMMA are 29 MPa [12], 75 MPa [12] and 25 MPa [27,62,63], respectively. The strain hardening modulus decreases linearly with the temperature for Polyamide B and Polyamide C, which is observed in literature by Engels and Van Melick with other polymers such as polycarbonate [12,59]. For Polyamide A, the strain hardening modulus seems no affected by temperature: there is no dependence to temperature.

Table 6. Hardening modulus E_{SH} in compression determined from the slope of the curves in the strain range 1.25–1.75 for the studied PPA.

Hardening modulus E_{SH} (MPa)	-20 °C	0 °C	23 °C	60 °C	100 °C	120 °C
Polyamide A	22.06	16.63	17.66	16.12	18.40	14.29
Polyamide B	/	20.15	18.17	15.14	11.86	7.95
Polyamide C	/	/	17.75	15.65	12.83	11.75

4. Conclusions

In this paper, the mechanical properties of polyphthalamides samples processed by injection molding have been investigated. The thermo-mechanical properties have been studied through DMTA experiments. All the studied PPA exhibit a characteristic dynamic mechanical response for a thermoplastic material. Three relaxations processes have been identified, denoted γ, β and α from the lower to the higher temperature. The impact properties were studied on a broad temperature range, using an instrumented Charpy impact test. The three PPA samples showed a brittle-ductile transition varying from a low energy dissipated during impact test to a high energy dissipated during impact of the order 130–160 kJ m^{-2}. At room temperature, the three PPA studied are brittle. They should be used for a composite application and thus improve their T_{bd}. The tensile and the compression behavior of three PPA with different degree of crystallinity have been studied. In tensile test, the PPA with the largest crystallinity is brittle at room temperature (Polyamide C), while the polyamide A and polyamide B are ductile. In both tests, we observed a strain hardening behavior, which is more pronounced in compression. The strain hardening regime in tensile test is influenced by the temperature as well as the amorphous or semi-crystalline character of the studied PPA. The measured strain hardening moduli in compression are around 18 MPa for the three PPA at 23 °C. The values of the E_{SH} modulus are relatively low compared to the PPO (75 MPa [12]). The strain hardening modulus is shown not to depend on crystallinity. Indeed, the strain hardening modulus E_{SH} of the semi-crystalline PPA, Polyamide C and Polyamide B, is found to be equal to the hardening modulus of the amorphous. Only the temperature has an influence on the strain hardening modulus E_{SH}: the strain hardening modulus decreases with increasing temperature. Strain hardening is a key feature for resistance to damage [11,64].

Declarations

Author contribution statement

Stéphanie Djukic, Anthony Bocahut, Jérôme Bikard, Didier R. Long: Conceived and designed the experiments; Performed the experiments; Analyzed and interpreted the data; Contributed reagents, materials, analysis tools or data; Wrote the paper.

Funding statement

This research did not receive any specific grant from funding agencies in the public, commercial, or not-for-profit sectors.

Competing interest statement

The authors declare no conflict of interest.

Additional information

The raw/processed data required to reproduce these findings cannot be shared at this time as the data also forms part of an ongoing study.

References

[1] M.I. Kohan, Nylon Plastics Handbook, Hanser Publishers, 1995. https://books.google.fr/books?id=oZibQgAACAAJ.
[2] C. Duval, Plastiques et automobile - D'hier à aujourd'hui, Techniques de l'Ingénieur 1 (2007). AM 3590.
[3] C. Duval, Plastiques et automobile - D'aujourd'hui à demain, Techniques de l'Ingénieur 1 (2007). AM 3591.
[4] M. Li, J. Bijleveld, T. Dingemans, Synthesis and properties of semi-crystalline poly(decamethylene terephthalamide) thermosets from reactive side-group copolyamides, Eur. Polym. J. 98 (2017).
[5] A.J. Uddin, Y. Ohkoshi, Y. Gotoh, M. Nagura, R. Endo, T. Hara, Melt spinning and laser-heated drawing of a new semiaromatic polyamide, PA9-T fiber, J. Polym. Sci. B Polym. Phys. 42 (2004) 433–444.
[6] T.F. Novitsky, C.A. Lange, L.J. Mathias, S. Osborn, R. Ayotte, S. Manning, Eutectic melting behavior of polyamide 10,T-co-6,T and 12,T-co-6,T copolyterephthalamides, Polymer 51 (2010) 2417–2425.
[7] C. Leboeuf, D.A. Harbourne, Synthesis of Semi-crystalline Polyphthalamides through Reactive Extrusion of Hexamethylene Terephthalamide Oligomer with Lower Melting, Semi-crystalline or Amorphous Polyamides, WO1999061509A1, 1999. https://patents.google.com/patent/WO1999061509A1/fr. (Accessed 1 April 2019).
[8] T. Cousin, J. Galy, J. Dupuy, Molecular modelling of polyphthalamides thermal properties: comparison between modelling and experimental results, Polymer 53 (2012) 3203–3210.
[9] G.P. Desio, Characterization and properties of polyphthalamide/polyamide blends and polyphthalamide/polyamide/polyolefin blends, J. Vinyl. Additive Technol. 2 (1996) 229–234.
[10] J.S. Lyons, Time and temperature effects on the mechanical properties of glass-filled amide-based thermoplastics, Polym. Test. 17 (1998) 237–245.
[11] L.E. Govaert, T.A.P. Engels, E.T.J. Klompen, G.W.M. Peters, H.E.H. Meijer, Processing-induced properties in glassy polymers, IPP 20 (2005) 170–177.
[12] H.G.H. van Melick, L.E. Govaert, H.E.H. Meijer, On the origin of strain hardening in glassy polymers, Polymer 44 (2003) 2493–2502.
[13] E.M. Arruda, M.C. Boyce, Evolution of plastic anisotropy in amorphous polymers during finite straining, Int. J. Plast. 9 (1993) 697–720.
[14] R.N. Haward, The application of a Gauss-Eyring model to predict the behavior of thermoplastics in tensile experiments, J. Polym. Sci. B Polym. Phys. 33 (1995) 1481–1494.
[15] T.A. Tervoort, L.E. Govaert, Strain-hardening behavior of polycarbonate in the glassy state, J. Rheol. 44 (2000) 1263–1277.
[16] A.R. Martins, A. Bocahut, M.-L. Michon, P. Sotta, Effect of intermolecular interactions on the viscoelastic behavior of unentangled polyamide melts, J. Rheol. 63 (2019) 377–389.
[17] P.J. Flory, Principles of Polymer Chemistry, Cornell University Press, 1953. https://books.google.fr/books?id=CQ0EbEkT5R0C.
[18] J. Brandrup, E.H. Immergut, E.A. Grulke, Polymer Handbook, fourth ed., Wiley, 2003. https://www.wiley.com/en-us/Polymer+Handbook%2C+2+Volumes+Set%2C+4th+Edition-p-9780471479369. (Accessed 1 April 2019).
[19] F.M. Preda, PhD Thesis, Dynamics of Polyamide in the Solid State in Presence of Solvents and in the Molten State, 1, Université Lyon, 2016.
[20] T.B. van Erp, L.E. Govaert, G.W.M. Peters, Mechanical performance of injection-molded poly(propylene): characterization and modeling, Macromol. Mater. Eng. 298 (2013) 348–358.
[21] C. Millot, Multi-scale Characterization of Deformation Mechanisms of Bulk Polyamide 6 under Tensile Stretching below and above the Glass Transition, PhD Thesis, INSA de Lyon, 2015.
[22] A.A. Griffith, The phenomena of rupture and flow in solids, Philos. Trans. R. Soc. Lond. - Ser. A Contain. Pap. a Math. or Phys. Character 221 (1921) 163–198.
[23] C. G'sell, J.M. Hiver, A. Dahoun, Experimental characterization of deformation damage in solid polymers under tension, and its interrelation with necking, Int. J. Solid Struct. 39 (2002) 3857–3872.
[24] M. Ponçot, F. Addiego, A. Dahoun, True intrinsic mechanical behaviour of semi-crystalline and amorphous polymers: influences of volume deformation and cavities shape, Int. J. Plast. 40 (2013) 126–139.
[25] J.L. Halary, F. Lauprêtre, L. Monnerie, Mécanique des matériaux polymères, 2008. Belin.
[26] A.I.H. Committee, ASM Handbook: Mechanical Testing and Evaluation, ASM International, 2000. https://books.google.fr/books?id=kEZLAQAAIAAJ.
[27] L.E. Govaert, T.A.P. Engels, M. Wendlandt, T.A. Tervoort, U.W. Suter, Does the strain hardening modulus of glassy polymers scale with the flow stress? J. Polym. Sci. B Polym. Phys. 46 (2008) 2475–2481.

[28] E. Baquet, Modélisation thermomécanique visco-hyperélastique du comportement d'un polymère semi-cristallin : application au cas d'une matrice polyamide 6.6, 2011. http://www.theses.fr/2011ENMP0101/document.
[29] A. Rios de Anda, L.-A. Fillot, D. Long, P. Sotta, Influence of the amorphous phase molecular mobility on impact and tensile properties of polyamide 6,6, J. Appl. Polym. Sci. 133 (2016) n/a-n/a.
[30] F. Beaume, B. Brulé, J.-L. Halary, F. Lauprêtre, L. Monnerie, Secondary transitions of aryl-aliphatic polyamides IV. Dynamic mechanical analysis, Polymer 41 (2000) 5451–5459.
[31] E. Laredo, M. Grimau, F. Sánchez, A. Bello, Water absorption effect on the dynamic properties of nylon-6 by dielectric spectroscopy, Macromolecules 36 (2003) 9840–9850.
[32] E. Laredo, M. Hernández, Moisture effect on the low- and high-temperature dielectric relaxations in nylon-6, J. Polym. Sci. Part B-Polymer Physics - J POLYM SCI B-POLYM PHYS. 35 (1997) 2879–2888.
[33] M. Laurati, P. Sotta, D.R. Long, L.-A. Fillot, A. Arbe, A. Alegrìa, J.P. Embs, T. Unruh, G.J. Schneider, J. Colmenero, Dynamics of water absorbed in polyamides, Macromolecules 45 (2012) 1676–1687.
[34] F. Beaume, F. Lauprêtre, L. Monnerie, A. Maxwell, G.R. Davies, Secondary transitions of aryl–aliphatic polyamides. I. Broadband dielectric investigation, Polymer 41 (2000) 2677–2690.
[35] F. Kremer, A. Schönhals, Broadband Dielectric Spectroscopy, 2003.
[36] J. Varlet, J.Y. Cavaillé, J. Perez, G.P. Johari, Dynamic mechanical spectrometry of nylon-12, J. Polym. Sci. B Polym. Phys. 28 (1990) 2691–2705.
[37] Y. Park, J. Ko, T.-K. Ahn, S. Choe, Moisture effects on the glass transition and the low temperature relaxations in semiaromatic polyamides, J. Polym. Sci. B Polym. Phys. 35 (1997) 807–815.
[38] Y. Shangguan, F. Chen, E. Jia, Y. Lin, J. Hu, Q. Zheng, New insight into time-temperature correlation for polymer relaxations ranging from secondary relaxation to terminal flow: application of a universal and developed WLF equation, Polymers (Basel) 9 (2017) 567.
[39] M.L. Williams, R.F. Landel, J.D. Ferry, The temperature dependence of relaxation mechanisms in amorphous polymers and other glass-forming liquids, J. Am. Chem. Soc. 77 (1955) 3701–3707.
[40] H.W. Starkweather, J.R. Barkley, The effect of water on the secondary dielectric relaxations in nylon 66, J. Polym. Sci. Polym. Phys. Ed 19 (1981) 1211–1220.
[41] A. Beneduci, Which is the effective time scale of the fast Debye relaxation process in water? J. Mol. Liq. 138 (2008) 55–60.
[42] G.D. Smith, R.L. Jaffe, Quantum chemistry study of conformational energies and rotational energy barriers in n-alkanes, J. Phys. Chem. 100 (1996) 18718–18724.
[43] K.B. Wiberg, M.A. Murcko, Rotational barriers. 2. Energies of alkane rotamers. An examination of gauche interactions, J. Am. Chem. Soc. 110 (1988) 8029–8038.
[44] A. Bocahut, J.-Y. Delannoy, D.R. Long, P. Sotta, Modeling molecular relaxation mechanisms in amorphous polymers: application to polyamides, Macromolecules 49 (2016) 1918–1932.
[45] C.A. Angell, Why C1 = 16–17 in the WLF equation is physical—and the fragility of polymers, Polymer 38 (1997) 6261–6266.
[46] J.D. Ferry, Viscoelastic Properties of Polymers, Wiley, 1980. https://books.google.fr/books?id=9dqQY3Ujsx4C.
[47] A. Rios de Anda, PhD Thesis, Influence of the Solvent Sorption, Additivation, and Chemical Modification on the Molecular Mobility Dynamics of Polyamide 6,6 Amorphous Phase and its Consequences on the Tensile and Impact Strength Properties of This Polymer, 1, Université Lyon, 2012, http://www.theses.fr/2012LYO10259/document.
[48] M. Louizi, V. Massardier, M. Taha, A. Ayoub, L. Vernhet, New routes of valorization of recycled and bio-sourced polyamides with a low toxicity process, Waste Biomass Valorization 4 (2013) 47–54.
[49] J.L. Halary, F. Laupretre, L. Monnerie, Polymer Materials: Macroscopic Properties and Molecular Interpretations, Wiley, 2011. https://books.google.fr/books?id=bqwgIXEZDeEC.
[50] L.E. Govaert, P. Timmermans, W.A.M. Brekelmans, The influence of intrinsic strain softening on strain localization in polycarbonate: modeling and experimental validation, J. Eng. Mater. Technol. Trans. Asme - J ENG MATER TECHNOL 122 (2000).
[51] A. Charvet, C. Vergelati, D.R. Long, Mechanical and ultimate properties of injection molded cellulose acetate/plasticizer materials, Carbohydr. Polym. 204 (2019) 182–189.
[52] JTA (Jules) Kierkels, Tailoring the Mechanical Properties of Amorphous Polymers, 2006.
[53] J. Richeton, S. Ahzi, L. Daridon, Y. Rémond, A formulation of the cooperative model for the yield stress of amorphous polymers for a wide range of strain rates and temperatures, Polymer 46 (2005) 6035–6043.
[54] C. G'Sell, J.M. Hiver, A. Dahoun, A. Souahi, Video-controlled tensile testing of polymers and metals beyond the necking point, J. Mater. Sci. 27 (1992) 5031–5039.
[55] J. Sweeney, P. Caton-Rose, R. Spares, P.D. Coates, Unified model of necking and shear banding in amorphous and semicrystalline polymers, J. Appl. Polym. Sci. 106 (2007) 1095–1105.
[56] J. Ye, S. André, L. Farge, Kinematic study of necking in a semi-crystalline polymer through 3D Digital Image Correlation, Int. J. Solid Struct. 59 (2015) 58–72.
[57] D.J.A. Senden, J.A.W. van Dommelen, L.E. Govaert, Strain hardening and its relation to Bauschinger effects in oriented polymers, J. Polym. Sci. B Polym. Phys. 48 (2010) 1483–1494.
[58] L. Monnerie, J. Halary, H. Kausch, Deformation, yield and fracture of amorphous polymers: relation to the secondary transitions, in: Advances in Polymer Science, 2005, pp. 215–372.
[59] T.A.P. Engels, L.E. Govaert, H.E.H. Meijer, The influence of molecular orientation on the yield and post-yield response of injection-molded polycarbonate, Macromol. Mater. Eng. 294 (2009) 821–828.
[60] M.C. Boyce, R.N. Haward, The post-yield deformation of glassy polymers, in: R.N. Haward, R.J. Young (Eds.), The Physics of Glassy Polymers, Springer Netherlands, Dordrecht, 1997, pp. 213–293.
[61] B.A.G. Schrauwen, R.P.M. Janssen, L.E. Govaert, H.E.H. Meijer, Intrinsic deformation behavior of semicrystalline polymers, Macromolecules 37 (2004) 6069–6078.
[62] J. Richeton, S. Ahzi, K.S. Vecchio, F.C. Jiang, A. Makradi, Modeling and validation of the large deformation inelastic response of amorphous polymers over a wide range of temperatures and strain rates, Int. J. Solid Struct. 44 (2007) 7938–7954.
[63] M. Wendlandt, T.A. Tervoort, U.W. Suter, Non-linear, rate-dependent strain-hardening behavior of polymer glasses, Polymer 46 (2005) 11786–11797.
[64] A. Charvet, Study of Mechanical Properties and Damage Mechanisms in Plasticized Cellulose Acetate Polymers, PhD Thesis, Université de Lyon, 2019.